Applied Geochemistry 100 (2019) 305–315

Contents lists available at ScienceDirect

Applied Geochemistry

journal homepage: www.elsevier.com/locate/apgeochem

Poregas distributions in waste-rock piles affected by climate seasonality and physicochemical heterogeneity

Bas Vriens*, Leslie Smith, K. Ulrich Mayer, Roger D. Beckie

Department of Earth, Ocean and Atmospheric Sciences, The University of British Columbia, 2020-2207 Main Mall, Vancouver, V6T 1Z4, Canada

ARTICLE INFO

Editorial handling by Prof. M. Kersten

Keywords:
Waste rock
Weathering
Poregas
Sulfide oxidation
Advection

ABSTRACT

The weathering of sulfide minerals in waste rock controls drainage water quality and water treatment requirements at mine sites. The availability of oxygen strongly affects the weathering rate of sulfidic waste rock but poregas distributions in heterogeneous, unsaturated waste-rock piles and the governing physical transport processes remain scarcely studied on practice-relevant scales. Here, we investigate the spatiotemporal variations in poregas in five large-scale, instrumented waste-rock piles (10,000 ± 2000 m^3) with different types of waste rock. Three piles with coarse, low-S waste rock exhibited atmosphere-like poregas compositions throughout, but two experimental piles with fine-grained, sulfide- and carbonate-rich waste rock contained localized hotspots with elevated temperatures, O_2 levels < 15%, and CO_2 concentrations > 2%. Oxygen depletion and CO_2 production from carbonate dissolution under acidic conditions was most pronounced during the wet season, when infiltrating precipitation strongly increased moisture content and repressed atmospheric gas exchange. Thus, spatial and temporal fluctuations in poregas were related to chemical reactivity and permeability of the waste rock as well as to seasonal climatic variations in hydrological transport. This study demonstrates that a quantitative understanding of these factors can lead to improved assessments of waste-rock weathering and drainage rates and therefore optimized design and management of waste-rock piles.

1. Introduction

In the process of extracting ore minerals, open pit mines generate large amounts of waste rock that is typically stored on-site in large, exposed waste-rock piles. The weathering of these (unsaturated) waste-rock piles may generate drainage with elevated acidity and metal concentrations that can have a deleterious impact on the downstream environment (Dold, 2014; Amos et al., 2015; Vriens et al., 2019). Therefore, it is important that mines are able to accurately forecast the volume, timing, and chemical characteristics of drainage originating from existing and future waste-rock stockpiles (Parbhakar-Fox and Lottermoser, 2015) and to design adequate water treatment facilities.

Many of the chemical reactions and physical transport processes controlling waste-rock weathering and drainage quality have been studied extensively over the past decades (Amos et al., 2015; Smith and Beckie, 2003; Nordstrom et al., 2015). In summary, the weathering of sulfidic waste rock consumes O_2 and water and produces heat, acidity and dissolved sulfate and metal ions, via:

$$MeS_2 + 3.5O_2 + H_2O \rightarrow 2H^+ + Me^{2+} + 2SO_4^{2-} \quad (1)$$

The acidity produced by sulfide oxidation can in turn be neutralized by the dissolution of silicate and carbonate minerals (when present) e.g., via:

$$2H^+ + CaCO_3 \rightarrow CO_2 + H_2O + Ca^{2+} \quad (2)$$

which produces carbon dioxide that tends to partition to the gas phase, particularly under acidic conditions. As a result, the oxidation of sulfide minerals (i.e. O_2 consumption) and dissolution of carbonate minerals (i.e. CO_2 production) in waste-rock piles can lead to temperatures and poregas pressures and compositions that are substantially different from atmospheric conditions (Lorca et al., 2016; Ritchie, 2003; Harries and Ritchie, 1985; Wels et al., 2003; Linklater et al., 2005). These temperature-, pressure-, and concentration gradients can trigger transport of O_2 into and of CO_2 out of the waste-rock piles, e.g., through diffusion, advection, or heat-induced convection (Smith and Beckie, 2003; Lorca et al., 2016; Ritchie, 2003; Harries and Ritchie, 1985; Vriens et al., 2018; Chi et al., 2013; Ning and Zhang, 1997; Amos et al., 2009; Lefebvre et al., 2001a,b,c). Field monitoring- and modeling studies have shown that O_2 consumption rates can exceed re-supply in piles containing reactive, sulfidic waste-rock, which leads to O_2 depletion that can ultimately limit oxidation rates and thus metal mobilization (Ritchie, 2003; Lefebvre et al., 2001a,b,c; Lahmira et al., 2017; Yanful

* Corresponding author.
E-mail address: bvriens@eoas.ubc.ca (B. Vriens).

https://doi.org/10.1016/j.apgeochem.2018.12.009
Received 15 October 2018; Received in revised form 5 December 2018; Accepted 6 December 2018
Available online 08 December 2018
0883-2927/ © 2018 Elsevier Ltd. All rights reserved.

Table 1
Summary of the installed instrumentation lines within the experimental waste-rock piles, with the major geochemical properties of the waste rock in the individual tipping phases indicated. Data from (Vriens et al., 2019).

	Location within pile	Particle sizes[a]				Elemental composition		Acid-Base-Accounting		
		d_{10}	d_{60}	C_u	C_c	C (%)	S (%)	AP[c]	NP[c]	NPR
Pile 1										
Line 1	Tipping phase 1	9	248	28	2	6.7	0.3	18	605	33
Line 2	Tipping phase 1 & 2[b]	11	275	25	2	4.5	0.7	20	392	19
Line 4	Tipping phase 2	18	370	21	2	2.2	1.1	33	180	5
Line 6	Protective layer	8	374	47	3	9.0	0.2	14	804	57
Pile 2										
Line 1	Tipping phase 1	0.13	29	223	8	0.1	2.1	70	10	0.98
Line 2	Tipping phase 2	0.11	18	164	5	0.2	0.8	20	8	0.40
Line 4	Tipping phase 3	0.13	24	185	4	0.0	2.0	49	7	0.14
Line 6	Protective layer	2	58	29	2	0.2	0.6	19	29	1.49
Pile 3										
Line 1	Tipping phase 1 & 2[b]	0.34	31	91	3	0.7	3.2	290	135	0.47
Line 2	Tipping phase 3	2	151	75	1	3.1	1.2	48	366	8
Line 4	Tipping phase 4	0.13	10	77	2	0.7	1.0	35	122	4
Line 6	Protective layer	2.7	81	30	3	1.0	2.2	78	126	2
Pile 4										
Line 1	Tipping phase 2	4	104	26	1	2.0	0.5	19	659	35
Line 2	Tipping phase 3	5	120	24	4	3.4	0.2	13	837	64
Line 4	Tipping phase 4	2	92	46	3	1.9	0.6	19	921	48
Line 6	Protective layer	6	105	17	1	1.9	0.5	28	558	20
Pile 5										
Line 1	Tipping phase 1 & 2[b]	9	92	10	1	0.8	0.9	25	566	23
Line 2	Tipping phase 3	10	104	10	1	2.2	0.1	21	575	27
Line 4	Tipping phase 4	2	120	51	4	2.6	0.3	14	742	53
Line 6	Protective layer	6	105	18	1	2.8	0.5	14	732	52

[a] Particle sizes: d_{10} and d_{60} are the intercepts, or particle sizes [mm], for the 10% and 60% fractions of the cumulative mass of the bulk waste rock, respectively. Further, C_u is the particle size uniformity coefficient, defined as d_{60}/d_{10}, and C_c is the particle size curvature coefficient, defined as $(d_{30})^2/(d_{10} \times d_{60})$.

[b] These instrumentation lines were installed in between two tipping phases. The given properties of the corresponding waste rock are averages for the two adjacent tipping phases.

[c] In [kg $CaCO_3$-eq. per 1000 kg waste rock].

et al., 1999; Elberling et al., 1994). In addition, previous studies have used O_2 consumption rates to deduce intrinsic sulfide oxidation rates in waste-rock piles (Vriens et al., 2018; Sracek et al., 2006). Accurate predictions of waste-rock weathering rates, and ultimately drainage quality, could thus benefit from a quantitative understanding of the *in-situ* poregas composition and gas transport mechanisms in waste-rock piles (Strömberg and Banwart, 1994; Malmström et al., 2000; Lahmira and Lefebvre, 2015; Lefebvre et al., 2001b; Birkham et al., 2003). Unfortunately, data on the temporal and spatial variability of poregas pressures and composition within large-scale waste-rock piles remains limited to date.

A few studies have previously monitored poregas composition in full-scale waste-rock piles (Harries and Ritchie, 1985; Vriens et al., 2018; Birkham et al., 2003; Lefebvre et al., 2001c). For instance, multilevel monitoring wells have been installed in boreholes in existing waste-rock piles to provide depth-discrete information on the poregas composition and related physical parameters, which can in turn be used to evaluate gas transport mechanisms (Ritchie, 2003; Vriens et al., 2018; Wels et al., 2003). However, abovementioned studies focused primarily on the distribution of O_2 and less on that of other pore gases like N_2, Ar, and CO_2. In addition, instrumented monitoring wells typically have a low spatial coverage and limited vertical resolution compared the spatial scales on which geochemical- and physical heterogeneities may occur in full-scale waste-rock piles.

At the Diavik mine in northern Canada, the construction of experimental piles facilitated the installation of automated gas monitoring systems with a comprehensive spatial coverage of the internal poregas pressures and composition (Chi et al., 2013; Amos et al., 2009; Smith et al., 2013). Data on the pressure variability within a waste-rock pile was used to show the relevance of wind-induced gas advection (Chi et al., 2013; Amos et al., 2009), but the O_2 and CO_2 concentrations in this pile remained near atmospheric levels due to low sulfide mineral weathering rates and high gas mobility. However, the poregas composition and gas transport processes in waste-rock piles will not only be affected by wind or temperature gradients (Chi et al., 2013), but also by variation in the geochemical composition of the waste rock (i.e. sulfide and carbonate content as discussed above) and the physical parameters that affect the porosity of the waste rock and thus air permeability/diffusivity (i.e. particle size and its distribution, and moisture content) (Vriens et al., 2018; Lefebvre et al., 2001b; Qing and Yanful, 2010). Unfortunately, the variability in these parameters can hardly be resolved on large spatiotemporal scales, and their combined influence on gas mobility and waste-rock weathering rates remains poorly quantified in full-scale heterogeneous waste-rock dumps.

In this paper, we investigate the spatial and temporal variation in poregas composition in five unique experimental waste-rock piles with different materials yet same geometry, and at the same location (i.e. climatic conditions) at Antamina mine in Peru. Building on previous work on the poregas composition in one of these piles (Lorca et al., 2016), the aim of this study was to examine how variations in poregas pressure and composition in waste-rock piles are affected by i) particle size and geochemical heterogeneity of the different waste rock materials, and ii) by climatic seasonality and related variations in moisture content in the waste rock.

2. Methods and materials

2.1. Construction of experimental waste-rock piles

Five experimental waste-rock piles (36 × 36 × 10 m; ~20,000 t of waste rock each) were constructed between 2006 and 2008 at the Antamina mine in Peru (9°31′59″S, 77°3′0″W; WGS84). The experimental piles were composed of run-of-mine waste rock and designed to represent the wide range of waste rock lithologies generated by

Antamina: the waste rock ranged from reactive sulfide-rich intrusive (pile 2) and skarn materials (pile 3) to less-reactive, carbonate-rich marbles (Pile 1), or a combination of these materials (Piles 4 and 5) (Vriens et al., 2019; Harrison et al., 2012; Love et al., 2004). The waste rock was end-dumped in distinct batches, or 'tipping phases', on top of a protective basal layer. The major geochemical properties of these tipping phases are summarized in Table 1; further details of the experimental waste-rock piles (e.g., waste rock mineralogy, particle size distributions) can be found elsewhere (Vriens et al., 2019). The climate at Antamina has a distinct wet and dry season (~80% of the annual 1200 mm precipitation falls between Nov-Apr), whereas the temperature is relatively constant throughout the year (~5 °C) (Blackmore et al., 2014).

2.2. Instrumentation for poregas sampling and analysis

Because the experimental piles were constructed by end-dumping distinct tipping phases, instrumentation lines could be installed within or in between the individual waste-rock batches in each of the experimental piles. This paper presents data from four of those instrumentation lines: lines 1, 2, and 4 located in or between individual tipping phases, and line 6, which was located in the protective basal layer above a thin saturated zone (see schematic in Fig. 1). Each instrumentation line contained five to seven temperature and volumetric water content sensors (ECHO-TE probes; Decagon Devices Inc.) and ten to thirteen poregas sampling ports (slotted 1.6 mm ID HDPE screens). The instrumentation lines were protected by flexible 4" corrugated HDPE tubes to prevent damage to the sensor cables and gas lines during further pile construction by end-dumping of waste rock.

A semi-automated gas analysis system was constructed using a GeoTech peristaltic pump (300 mL min^{-1}) and a solenoid-controlled switchboard equipped with timer-controlled valves. Connected to the ~50 sampling ports of one experimental waste-rock pile at a time, the system alternately pumped poregas from the various sampling ports through HDPE tubing and a Genie membrane filter (Model 120, A + Corporation) to remove moisture into: i) an infrared CO_2 analyzer (model LI-820, Li-Cor Biosciences), ii) a galvanic O_2 sensor (model SO-200, Apogee Instruments), and iii) a differential pressure transducer (Setra model 264) coupled to a Campbell CS106 barometer to record atmospheric pressure under no-flow conditions. The switchboard was programmed so that differential pressure between a selected port and ambient air was measured under no-flow conditions, taking measurements about once every 3 min while sequentially cycling from port to port so that virtually continuous records were collected. The differential pressure measurements were interrupted once per day for CO_2 and O_2 analyses in each sampling port, which was done after purging each sampling port and gas line for > 2 min to ensure representation of *in-situ* conditions (Lorca et al., 2016). The CO_2 analyzer measured between 0 and 22,000 ppm (~2.2 v/v-%), whereas O_2 was measured between 0 and 100 v/v-%. The functioning and accuracy of the poregas O_2 and CO_2 sensors were regularly verified using compressed air (380 ppm CO_2, 20.95% O_2) and a fixed-composition calibration gas (1.5% CO_2, 98.5% N_2, Praxair), both of which were also automatically drawn by the gas collection system from gas cylinders. All temperature, moisture content, gas pressure and -composition data was stored on Campbell CR1000 dataloggers and periodically retrieved.

Additional poregas samples were manually collected through the existing gas sampling ports on the switchboard that were connected to instrumentation lines 1, 2, 4, and 6 using gas-tight syringes (Hamilton). Collected poregas samples were transferred into pre-evacuated 10 mL borosilicate ampules that were crimp-sealed with dual-layer PTFE/silicon septa, and transported to the laboratory. The concentrations of O_2, N_2, Ar, and CO_2 were determined on a Varian CP-4900 dual channel gas chromatograph equipped with surface-micromachined TCD detectors. Using He as a carrier gas, Ar, O_2, and N_2 were separated using a MolSieve 5A PLOT capillary column, whereas a PoraPLOT-U column was used to isolate CO_2 (Agilent). The instrument was regularly calibrated with ambient air and with Supelco calibration standard #234, which consisted of 5% N_2, 5%O_2, and 5% CO_2 in He.

2.3. Data collection and processing

The semi-automated gas sampling system could be connected to the gas sampling ports of one experimental waste-rock pile at a time. Therefore, sensor-based *in-situ* measurements of temperature, moisture content, and poregas CO_2 and O_2 concentrations were first collected for all five experimental piles in April 2010 (i.e. at end of the wet season at Antamina; drain-down of the waste rock), by deploying the gas sampling system sequentially at each of the five experimental piles for 1 week at a time. No poregas pressure data was collected at this time due to sensor malfunction. The spatial variability of the other aforementioned parameters was examined by plotting contour 'snapshots' of the average conditions measured during that one-week period. These contour plots were constructed using a Gaussian process regression method ('Kriging') using the OriginPro software (OriginLab), setting atmospheric conditions as boundaries for the exposed slopes but no boundaries for the occluded (posterior and basal) faces of the pile.

Subsequently, the automated gas sampling system was moved to experimental waste-rock pile 2 (containing the most reactive waste rock) between April 2010 and January 2011 to record temporal changes in poregas temperature, pressure, and composition. A portion of this temporal data has been previously published elsewhere (Lorca et al., 2016), and is complemented in this paper by additional (and more spatially-resolved) poregas-temperature, -moisture content, and -composition data, as well as poregas-pressure data, recorded for the most frontal region of waste-rock pile 2 (instrumentation line 4).

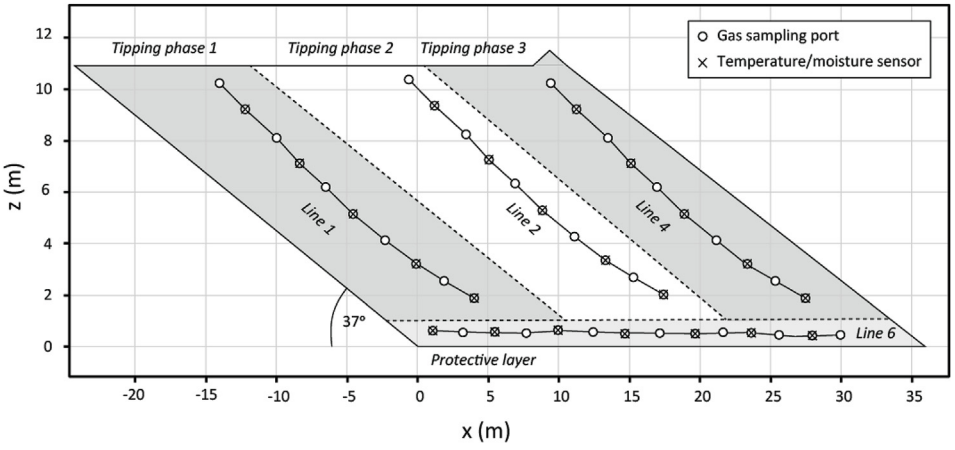

Fig. 1. Schematic cross-sectional illustration of the dimensions and approximate locations of the instrumentation lines within the experimental waste-rock piles (exaggerated vertical scaling). Gas sampling ports and temperature/moisture sensors were installed in an alternating pattern along the instrumentation lines in each waste-rock tipping phase and in the protective basal layer as indicated.

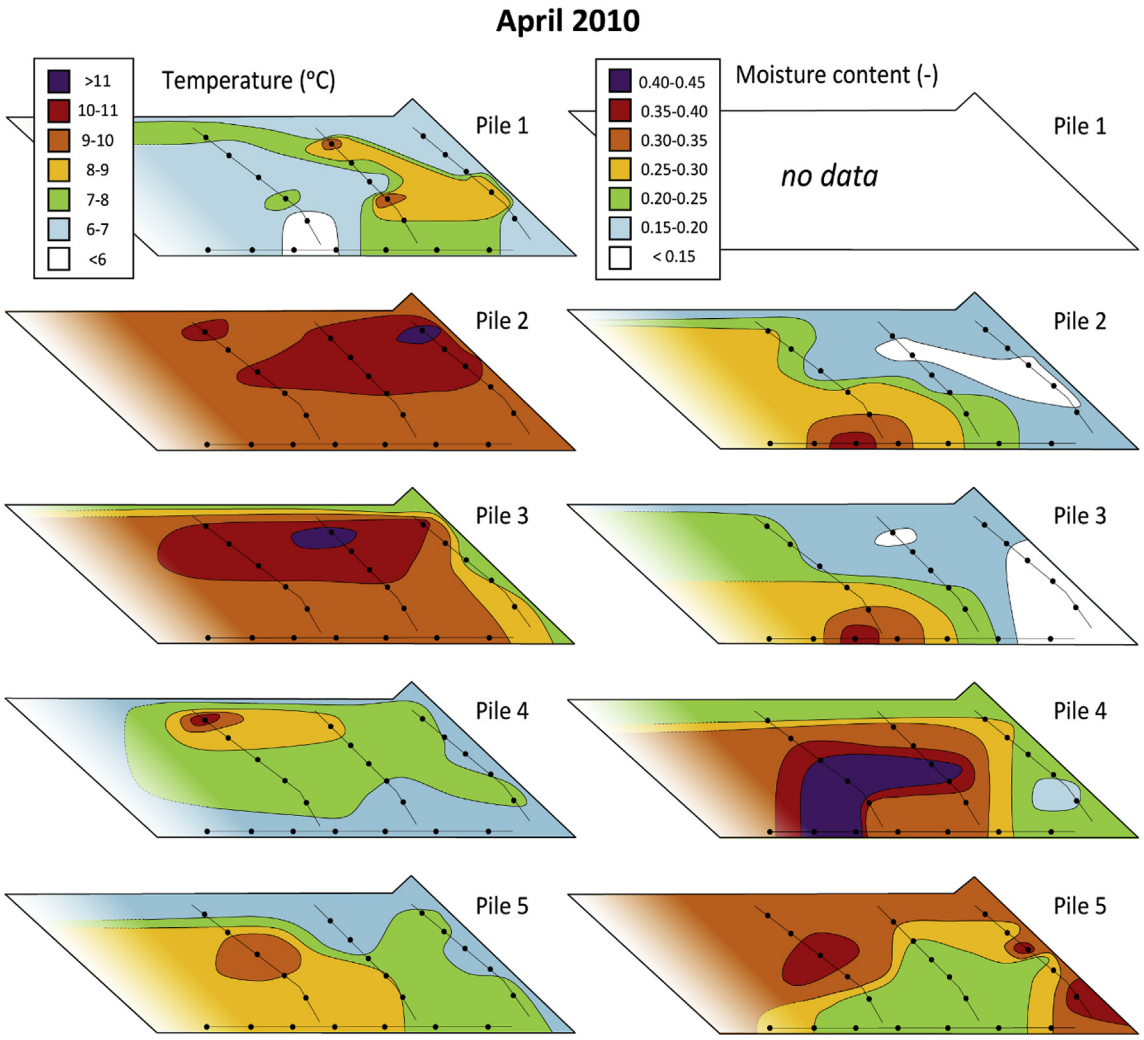

Fig. 2. Schematic (cross-sectional) illustration of the spatial variability of the waste-rock poregas temperature (left) and moisture content (right) in the experimental waste-rock piles. The visualized data represents averages for April 2010 (i.e. at the end of the wet season). No moisture content data for pile 1 was obtained due to sensor malfunction. The black lines and dots indicate approximate locations of the instrumentation lines and temperature/moisture sensors.

Finally, manual poregas samples were collected during a field campaign in December 2010 from experimental piles 3 and 5. During that time, the automated gas sampling system was also temporarily moved to experimental waste-rock piles 3 and 5 to measure differential poregas pressures. The obtained poregas composition- (including N_2 and Ar) and poregas pressure data was similarly evaluated by drawing contour 'snapshots' for piles 3 and 5 for December 2010, as described above.

3. Results and discussion

3.1. Heterogeneous distribution of heat and moisture

Sensor measurements revealed a heterogeneous distribution of heat and moisture in all experimental waste-rock piles in April 2010, with irregularly localized hotspots of elevated temperature and moisture (Fig. 2). The internal temperatures recorded in all experimental waste-rock piles generally exceeded ambient air temperatures (~6 °C in April 2010), and 'hotspots' with elevated temperatures could be observed in all experimental piles (although less pronounced in those piles with less reactive waste rock). Whereas experimental piles 1, 4, and 5 exhibited only marginally elevated temperatures of up to 8 °C and contained only small hotspots > 9 °C, experimental piles 2 and 3 were consistently warmer than 9 °C, and had large areas that were warmer than 10 °C, i.e. more than 4 °C above average local air temperatures (Fig. 2). Due to the relatively constant annual air temperatures, little seasonal oscillation in the internal pile temperatures was observed (data not shown).

The recorded waste rock temperature gradients are relatively small compared to observations in other and larger waste-rock piles with similarly reactive waste rock (Harries and Ritchie, 1985; Lefebvre et al., 2001b; Birkham et al., 2003), suggesting reduced sulfide reactivity and/or effective heat transfer between the mesoscale experimental piles and their surroundings. Furthermore, a typical insulated internal thermal regime as observed e.g., in a similarly sized low-S experimental pile at the Diavik mine in the Canadian Arctic (Pham et al., 2013) could not be discerned in any of the piles in April 2010 due to the heterogeneous heat generation from reactive hotspots. These examples illustrate that the heat distribution and thermal regimes in waste-rock piles may differ greatly as a function of waste rock properties, pile design and dimensions, and local climate.

The waste rock in experimental piles 2 and 3 contained significantly less moisture than the waste rock in experimental piles 4 and 5 in April 2010 (moisture content data for experimental pile 1 was not collected due to sensor malfunction). Experimental piles 2 and 3 also contained finer-grained waste rock (Table 1), so that their reduced moisture content may also be related to lower porosity. The moisture content sensor measurements revealed a typically dryer waste rock near the exposed surfaces of experimental piles 2, 3, and 4, and a wetter interior

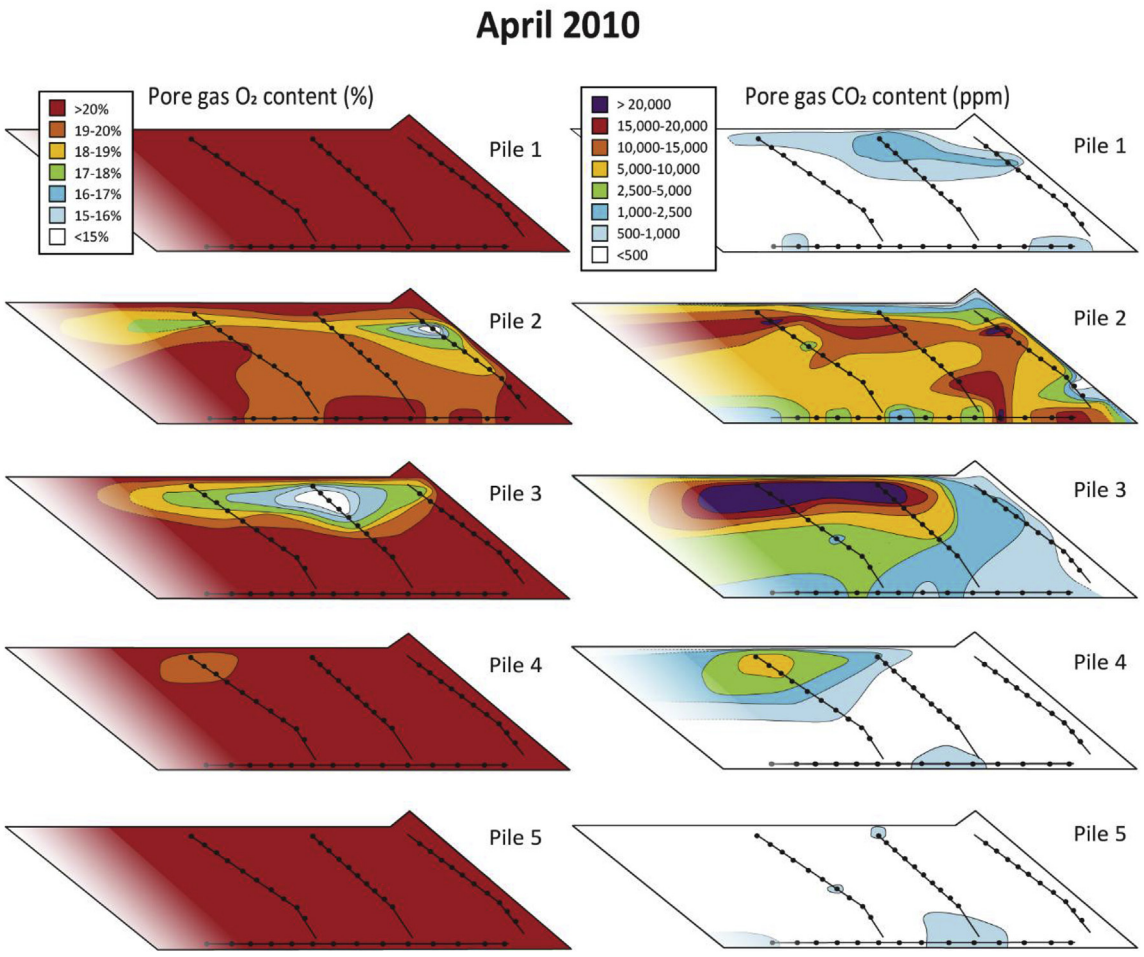

Fig. 3. Schematic (cross-sectional) illustration of the spatial variability of the poregas composition (O_2, left, and CO_2, right) in the experimental waste-rock piles. The visualized data represents averages for April 2010 (i.e. at the end of the wet season). The black lines and dots indicate the approximate location of the instrumentation lines and gas sampling ports.

in those piles (Fig. 2) in April 2010. In contrast, experimental pile 5 exhibited a relatively dry interior compared to wetter outer peripheries during that time. There appeared to be little overlap between the spatial distribution of temperature and moisture content, and hotspots of elevated temperatures and moisture content were observed in different locations (i.e. front, back, top, and bottom) within the experimental piles. The five experimental piles thus exhibited widely different temperature and moisture content distributions with considerable internal variability.

3.2. Spatially variable poregas compositions

Similar to the observed temperature and moisture content distributions, poregas compositions in the experimental piles were highly different and spatially variable as well (Fig. 3). By the end of the wet season in April 2010, poregas O_2 concentrations throughout experimental piles 1, 4, and 5 remained > 20%, i.e. at practically atmospheric levels, whereas experimental piles 2 and 3 developed significant hotspot zones in which O_2 content dropped < 15% (Fig. 3). Similarly, sensor-based CO_2 measurements indicated that most of the waste rock of experimental piles 1, 4, and 5 contained negligible CO_2 (< 500 ppm), whereas piles 2 and 3 contained hotspots with elevated CO_2 levels > 22,000 ppm (> 2.2%), i.e. exceeding the upper detection limit of the CO_2 sensor (Fig. 3). These CO_2 concentrations agree with previously measured CO_2 levels in waste rock with elevated sulfide- and carbonate content (i.e. several % CO_2 (Harries and Ritchie, 1985; Birkham et al., 2003)) and previous research in a full-scale dump at Antamina showed that CO_2 levels in similar waste rock can reach > 7% (Vriens et al., 2018). The distribution patterns of O_2 and CO_2 were highly anti-correlated, with elevated CO_2 hotspots occurring only in regions that exhibited O_2 depletion (Fig. 3). This high degree of anti-correlation suggests fast reaction versus relatively slow atmospheric exchange rates, particularly during the end of the wet season in April 2010. Finally, zones with both significant O_2 depletion and CO_2 production were correlated to elevated temperatures but not moisture content (compare Figs. 2 and 3).

Investigation of the poregas compositions in piles 3 and 5 in December 2010 using the manually collected poregas samples reveals that poregas O_2- and CO_2 levels quantitatively agree with those measured in April 2010 and at the same time show a spatial distribution similar to that measured in April 2010 (Fig. 4): experimental pile 5 appears completely oxygenated with atmospheric O_2 levels (> 20%) and low CO_2 content (< 1000 ppm), whereas experimental pile 3 exhibited a significant area near the top of the pile's center that was O_2-depleted (< 16%) and CO_2-enriched (> 10,000 ppm). From the additional analysis of poregas samples from experimental piles 3 and 5, some temporal variation in poregas composition in those piles becomes apparent: whereas pile 5 only exhibited slightly more CO_2 in December 2010 compared to April 2010, pile 3 showed a significant decrease in the extent of O_2 depletion and CO_2 accumulation in December 2010 compared to April 2010.

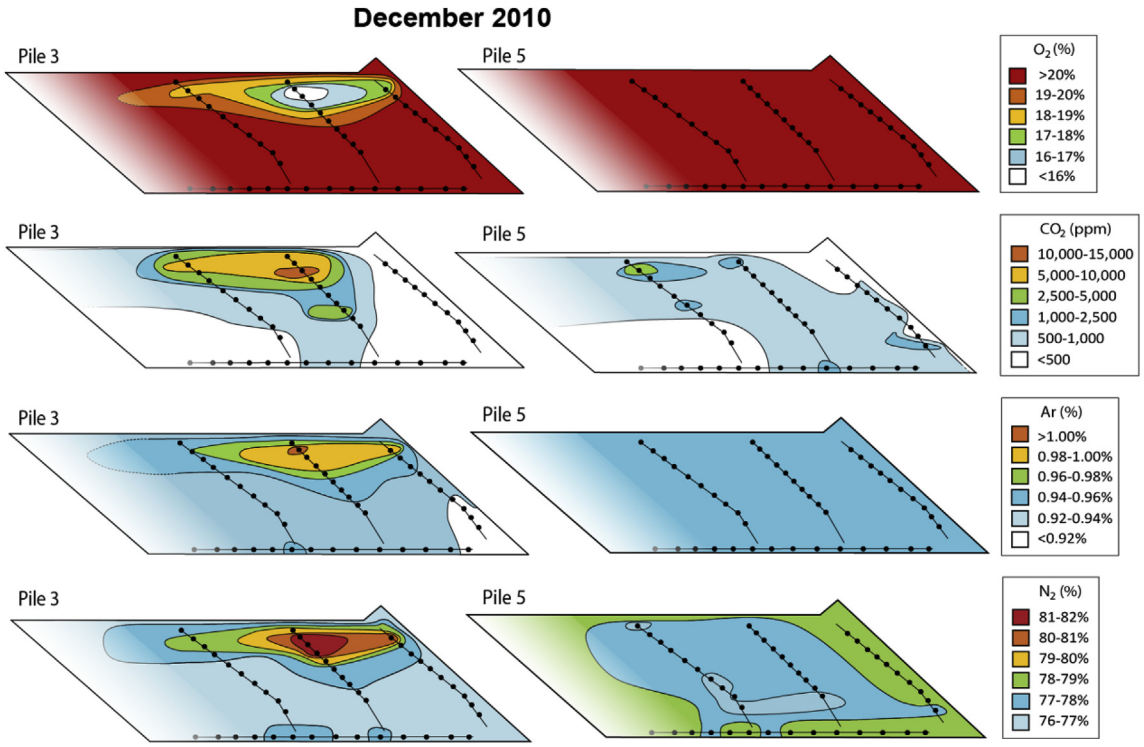

Fig. 4. Schematic cross-sectional illustration of the spatial variability of the poregas composition (from top to bottom: O_2, CO_2, Ar, and N_2) in experimental waste-rock piles 3 (left) and 5 (right). The visualized data represents one-time measurements in December 2010, i.e. early in the wet season. The black lines and dots indicate the location of the instrumentation lines and gas sampling ports.

3.3. Indications of gas transport limitations

In December 2010, i.e. early in the wet season, poregas Ar and N_2 concentrations were relatively homogenous and near atmospheric levels throughout experimental pile 5, whereas experimental pile 3 contained an area with relatively enriched Ar and N_2 levels that coincided with local O_2 depletion and CO_2 enrichment (Fig. 4). Relative to the average atmospheric composition, O_2 depletion in the reactive zone in experimental pile 3 was approximately 4%, which was contrasted by relative enrichments of CO_2 (~1%), N_2 (~3%) and Ar (~0.07%). Assuming that the waste-rock pile is an open system, the observed enrichment of conservative gases N_2 and Ar relative to the average atmospheric composition may be indicative of advective gas transport into this reactive zone (Molins and Mayer, 2007).

Investigation of the poregas pressures during the manual poregas sampling in December 2010 showed that the average differential poregas pressures in experimental pile 5 oscillated only slightly between −2.5 Pa and +2.5 Pa relative to external barometric pressures, whereas experimental pile 3 exhibited negative average differential poregas pressures down to −15 Pa near the crown of the pile and elevated average differential poregas pressures up to +12 Pa in its basal region (Fig. 5). These average differential poregas pressures are comparable to e.g., pressure vectors measured in a similarly sized waste-rock pile at the Diavik mine (Chi et al., 2013; Amos et al., 2009), and demonstrate that small but relevant net pressure gradients may be identified in waste-rock piles on top of daily pressure fluctuations (on the order of 20 Pa as a result of temperature variation; data not shown). The smaller pressure gradients observed in experimental pile 5 are consistent with the near-atmospheric poregas composition in that pile (Fig. 4) and the fact that experimental pile 5 was composed of coarse-grained, highly air-permeable waste rock (Table 1). In turn, the more significant negative differential pressures recorded near the crown of experimental pile 3 overlap with its reactive zone where significant depletion of O_2 and enrichment of N_2 and Ar was observed (Fig. 4), and thus provide a further indication of advective transport into this poorly permeable region. The positive differential pressures recorded at the bottom of pile 3 may be a result of higher moisture content in that area due to infiltrating precipitation (Fig. 2), but require further quantitative investigation. In summary, the presented results suggest that O_2 consumption in the reactive zone in experimental pile 3 led to significant changes in poregas composition (e.g., increased relative abundance of N_2 and Ar) and an associated reduction in poregas pressure that may have triggered advective O_2 transport into the pile. Other transport mechanisms may have contributed to O_2 re-supply (e.g., diffusion, wind-driven advection, thermal convection), but O_2 re-supply into the reactive zone was clearly insufficient to keep poregas O_2 concentrations near atmospheric levels and may therefore be expected to limit sulfide oxidation rates in reactive zones in experimental piles 2 and 3.

3.4. Estimation of sulfide oxidation rates

In an approach similar to (Harries and Ritchie, 1981) and (Pham et al., 2013), the thermal profiles within the studied waste-rock piles may be used to estimate apparent sulfide oxidation rates. A heat budget for an experimental waste rock pile can be defined based on the conservation of heat:

$$\text{Net heat outflow} = \text{heat generation} - \text{heat storage} \quad (3)$$

No significant net warming or cooling of the piles was observed during the study period (data not shown) and this minimal temporal variation in internal pile temperatures likely results from similarly stable ambient air temperatures (Vriens et al., 2019). Because all piles were consistently warmer than ambient temperatures, it is assumed that this unidirectional temperature gradient reflects a *steady-state* heat transfer and that the net heat storage in the piles equals 0. Consequently, the net heat generation rate within the pile may be estimated from the net heat outflow rate. When one assumes that the main heat transfer mechanisms are conduction and convection (i.e. no radiative

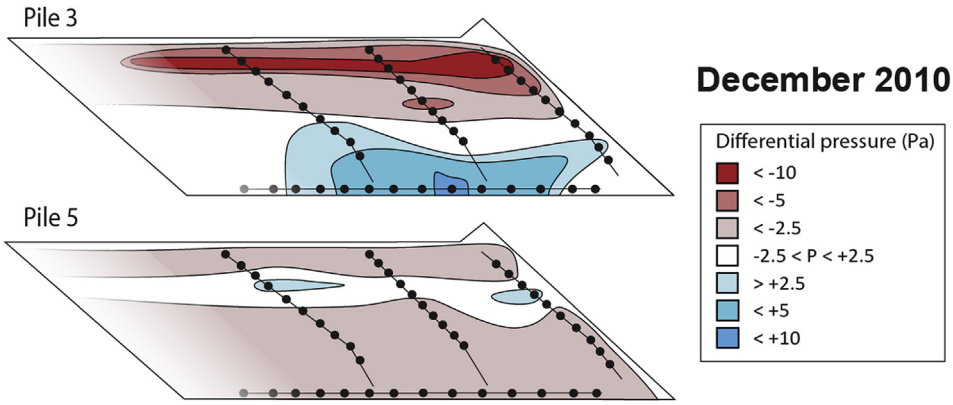

Fig. 5. Schematic cross-sectional illustration of the spatial variability of the differential poregas pressures in experimental waste-rock piles 3 (left) and 5 (right) in December 2010. The contour plot was constructed based on average differential pressures calculated for each of the poregas sampling ports, based on ~20 sensor measurements collected in December 2010, i.e. early in the wet season. The black lines and dots indicate the location of the instrumentation lines and sensors.

heat transfer and (latent) heat effects from infiltrating or evaporating pore water), and that the waste rock is homogenous and isotropic with respect to thermal properties, the mean heat outflow, q [W m^{-2}], may be described using (Welty et al., 1984):

$$q = -\lambda_{wr}\frac{\partial T}{\partial x} + u_x \rho_{air} c_{air} T \quad (4)$$

in which λ_{wr} is the bulk thermal conductivity of the waste rock (between 1.2 and 2.1 [W °C^{-1} m^{-1}] for waste rock in piles 1, 4, and 5 and waste rock in piles 2 and 3, respectively, assuming constant and homogeneous moisture content), $\partial T/\partial x$ is the observed temperature gradient [°C m^{-1}], ρ_{air}, c_{air}, and T are the air density (0.75 [kg m^{-3}], assumed constant), specific heat of air (~1000 J kg^{-1} °C^{-1}), and bulk air temperature (5 °C), respectively, under the conditions at Antamina, and u_x is the advective air velocity [m s^{-1}], which can be estimated using Darcy's law for gas (Massmann and Farrier, 1992; Thorstenson and Pollock, 1989):

$$u_x = -\frac{K}{\mu}\left(\frac{\partial P}{\partial x} + \rho_{air} g\right) \quad (5)$$

in which K is the net air permeability (assumed to vary between 1×10^{-13}-1×10^{-11} [m^2], depending on the grain size of the waste rock in the piles (Vriens et al., 2018), μ is the dynamic viscosity of the air under the conditions at Antamina (1.7×10^{-5} [kg m^{-1} s^{-1}], assumed to be constant), $\partial P/\partial x$ is the observed pressure gradient [Pa m^{-1}], and g is the gravitational acceleration (9.81 [m s^{-2}]).

The bulk internal temperatures in the experimental piles, averaged over all sensor locations, varied from 7.1 °C (pile 1) to 10.2 °C (pile 2; Fig. 2), and, as mentioned before, did not significantly vary over time. In a simplified scenario, heat conduction may subsequently be assumed to be directed out of the pile from all its faces (i.e. top, bottom, front, back, and flanks, totaling 3820 m^2), when a constant 'background' temperature of 5 °C is set. Convective heat transfer will only take place at the exposed faces of the pile (i.e. top, front, and flanks, total 1890 m^2), and, at average pressure differences of maximally 10 Pa m^{-1} (see above), will be at most 10% of the conductive heat transfer. Taken together, average heat generation rates ranging between 1500 [W] (pile 1) and 9500 [W] (pile 2) can be calculated for the experimental piles. Assuming that the only source of heat is exothermic heat release from pyrite oxidation (~1500 kJ mol^{-1}), and using the total masses of each experimental pile (Vriens et al., 2019), these heat generation rates suggest sulfide oxidation rates varying between 0.05 and 0.3 g S kg^{-1} waste rock yr^{-1} for the five experimental waste-rock piles. These rates are on the higher end of sulfide oxidation rates deduced from previous monitoring of the drainage chemistry from the same experimental waste-rock piles (ranging from 0.1 g S kg^{-1} waste rock yr^{-1} in the reactive, fine-grained waste rock of piles 2 and 3, to 0.01 g S kg^{-1} waste rock yr^{-1} in the less reactive, coarse waste rock of piles 1, 4, and 5) (Vriens et al., 2019), but fall within the broad range of oxidation rates that were calculated based on previous poregas monitoring in experimental pile 2 (ranging from 0.001 to 1 g S kg^{-1} waste rock yr^{-1} for occluded, basal waste-rock, and exposed, reactive waste-rock, respectively (Lorca et al., 2016)). Further, these oxidation rates are in the same order of magnitude than rates observed from column experiments (e.g., < 5 g S kg^{-1} waste rock yr^{-1}) (Strömberg and Banwart, 1999) and rates used in model simulations (< 1 g S kg^{-1} waste rock yr^{-1}) (Linklater et al., 2005).

3.5. Role of geochemical and physical heterogeneities

The observed heat and CO_2 generation and O_2 depletion in large sections of experimental piles 2 and 3 (Figs. 2 and 3) is consistent with the presence of more reactive and finer-grained waste rock in these piles: waste rock in experimental piles 2 and 3 had relatively elevated acid production potential (i.e. high S-content) and little neutralization potential (i.e. low C-content) compared to the other experimental piles (Table 1). Furthermore, experimental pile 2 had waste rock with very low carbonate content, whereas pile 3 contained carbonate-richer waste rock, which matches a higher CO_2 production in pile 3 compared to pile 2 (Fig. 3). These agreements support the general notion that bulk poregas composition and temperatures in waste rock are mainly controlled by the geochemical reactivity of the waste rock, which is illustrated by their correlations to the net-neutralizing potential ratio (NPR) of the bulk waste rock (Fig. 6). Two exceptions may be noted: i) no significantly elevated CO_2 and temperatures or decreased O_2 levels were observed in tipping phase 2 (instrumentation line 4) of experimental pile 1, albeit a small NPR, and ii) sub-atmospheric O_2 levels and slightly elevated CO_2 content and temperatures were recorded in the uppermost region of tipping phase 1 (instrumentation line 1) in experimental pile 4, although the bulk composition of this waste rock did not indicate significant reactivity (compare Table 1 and Figs. 2 and 3). These minor anomalies (designated in Fig. 6) may be explained by: i) grain-size effects or the presence of localized hotspots of reactive waste rock whose weathering induced local non-atmospheric gas compositions but whose reactivity was averaged in the bulk waste-rock characterization, and ii) by fast heat- and air exchange with the atmosphere compared to relatively slow sulfide oxidation- and carbonate dissolution kinetics. Previous research has shown that small-scale variations in waste rock reactivity resulting from grain-size effects or mineralogical heterogeneity may cause drainage qualities different than expected from bulk waste-rock characterization (Gerke et al., 1998; Pedretti et al., 2017; Blackmore et al., 2018). Our results illustrate that such effects thus also pertain to the (local) poregas distribution in waste-rock piles, which needs to be considered when using analyses of local poregas samples to quantify *in-situ* weathering rates.

The poregas distribution in waste-rock piles will, in addition to geochemical reactivity, also be linked to the particle size of waste rock: a reactive mineral surface area increases with decreasing particle size (Strömberg and Banwart, 1999), and the transport of air through finer-

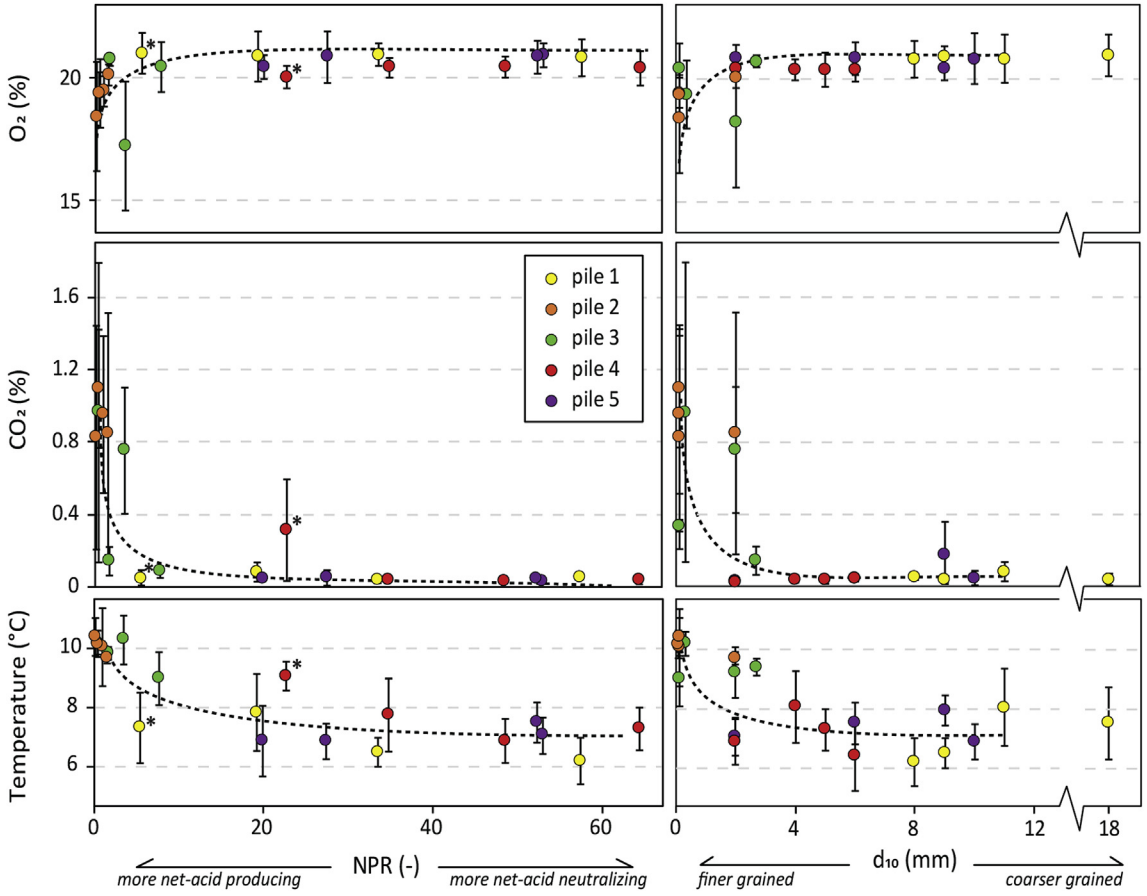

Fig. 6. Correlations between the poregas composition and temperatures measured in the five experimental piles and the average reactivity (as NPR, left) and particle size (as d_{10}, right) of waste rock in these piles. Poregas composition and temperature data collected in April 2010 was averaged for each instrumentation line (4 per pile; error bars indicate standard deviation from the 5 sensors in each instrumentation line) and compared to the corresponding net-acid neutralizing potential ratio (left) and particle size (right) of that waste rock (Table 1). The particle size is expressed as d_{10}, i.e. the particle diameter that 10% of the waste rock is smaller than (right). Major trends, for illustrative purposes only, are indicated by the dashed lines; 'outliers' discussed in the text are indicated by the asterisks. The legend applies to all frames.

grained waste rock is slower than through coarse waste rock (i.e. reduced porosity and air permeability will cause lower rates of O_2 resupply or CO_2 outgassing). This effect of particle size on the poregas distribution in the studied experimental piles is illustrated by: i) the smaller differential pressure gradients observed in the porous waste-rock of experimental pile 5 compared to the finer-grained, less permeable waste rock of pile 3 (Fig. 5), ii) the inverse correlation between waste rock particle size and the extent by which poregas compositions deviate from the atmospheric composition (Fig. 6), or iii) the fact that O_2 depletion and elevated CO_2 concentrations and temperatures were typically observed in the upper regions of the experimental piles (Figs. 2 and 3), which contain finer-grained waste rock due to the fining-upward sorting induced by the end-dumping technique used to construct the experimental piles. The different poregas compositions and distributions observed within the experimental piles thus appear strongly related to both the waste rock geochemistry and particle size.

3.6. Temporal variations in poregas composition

Temporal changes in the poregas compositions of experimental piles 3 and 5 can be inferred by comparing sensor-based analyses and manually collected poregas sample measurements from April and December 2010, respectively (Figs. 3 and 4). This demonstrates that significant variation in poregas composition may result from factors other than the chemical reactivity or particle size of the waste rock, which may be assumed to be temporally stable. In this section, the temporal variability in poregas compositions will be discussed for the reactive zone in pile 2, which exhibited the largest observed seasonal variations.

Between April 2010 and November 2010 (i.e. the dry season of 2010), a drain-down of experimental pile 2 occurred, as evidenced by declining moisture contents (Fig. 7) or the outflow hydrograph (published elsewhere (Vriens et al., 2019)). With the onset of the wet season in November 2010, the waste-rock pile wetted up and several rapid responses to significant precipitation events could be identified throughout the pile. The observed moisture contents at different depths suggest the advancement of a wetting front through the pile (Fig. 7): sensors near the top surface of the pile increased significantly in moisture content by the end of October, whereas the wetting front reached sensors in the center and deeper parts of the pile by mid-December. In concurrence with these variations in moisture content, strong seasonal variations in the poregas composition were observed (Fig. 7): O_2 concentrations increased and CO_2 levels and differential poregas pressures declined towards atmospheric conditions during the dry season, suggesting enhanced gas exchange between the waste rock and the atmosphere with drier conditions. The waste rock moisture content, even in the dry season, never dropped < 0.05, indicating that residual water is effectively retained in the finer fractions, and that water-availability limitations on the intrinsic oxidation rates will be minimal. With the onset of the wet season, O_2 depletion occurs and CO_2 starts to build up throughout the pile as the waste rock wets up. Concurrently, the poregas pressures near the reactive zone decrease up to

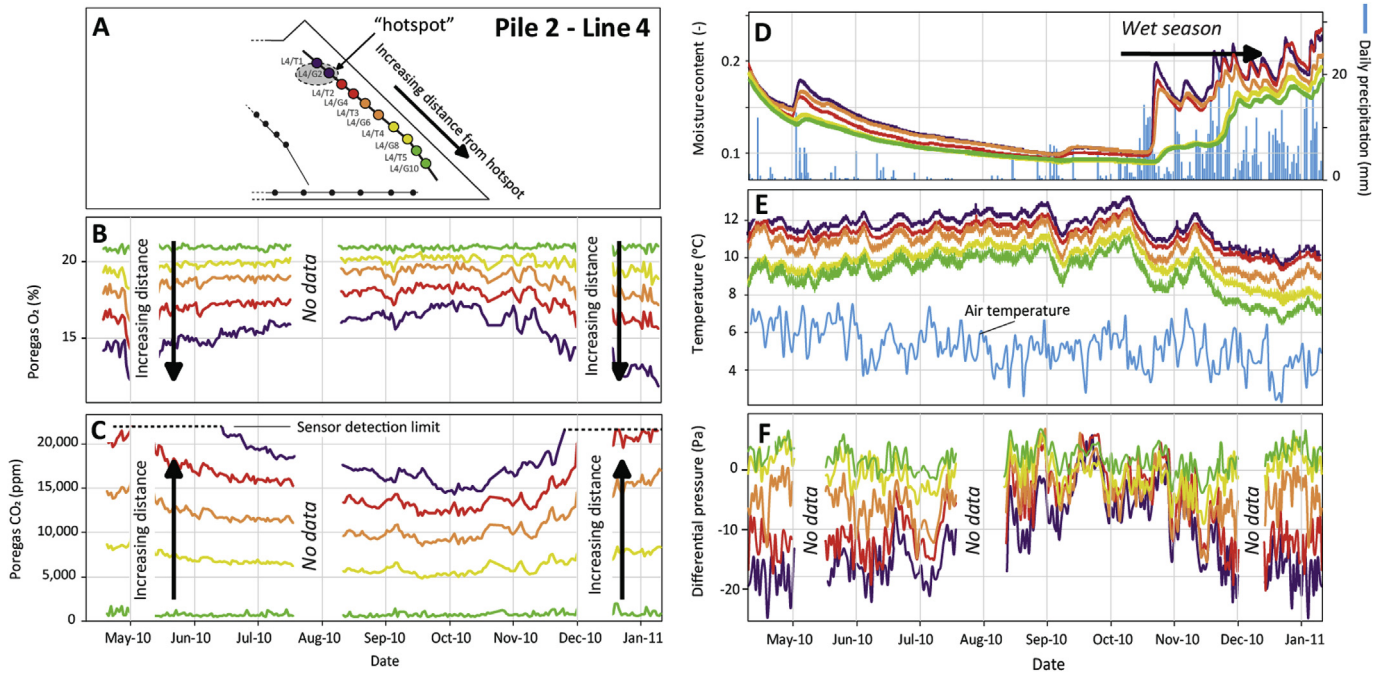

Fig. 7. Temporal variation in poregas composition, temperature, pressure, and moisture content recorded in waste rock located in the reactive zone in the front of experimental pile 2 between April 2010 and February 2011. The various frames show: (**a**) the location of instrumentation line 4 and corresponding sensors in experimental pile 2, and the location of the reactive 'hotspot' area, (**b**) the temporal variation of poregas O_2 content, (**c**) CO_2 content, (**d**) moisture content, (**e**) temperature, and (**f**) differential pressure (20 point moving average) between April 2010 and February 2011. The color coding of the plotted time series corresponds to the sensor locations indicated in frame **a**, with the increasing distance from the 'hotspot' indicated in frames **b** and **c**. Average daily precipitation and air temperatures are indicated in frames **d** and **e**, respectively. Data in frames **b**, **c**, **d**, and **e** was adapted from (Lorca et al., 2016). (For interpretation of the references to color in this figure legend, the reader is referred to the Web version of this article.)

−20 Pa relative to atmospheric conditions. This suggests that an increasing moisture content in the waste rock causes partial sealing of the gas migration pathways and inhibits O_2 and CO_2 transport. In other words, increasing moisture content reduces the gas-filled pore space and connectivity of gas migration pathways, inhibiting O_2 ingress and CO_2 loss to the atmosphere: O_2 diffusion is orders of magnitude lower through water than through air, and advective air transport slows down when infiltrating precipitation reduces the air permeability of the waste rock until advection virtually stops at porewater saturations > 80% (Lahmira et al., 2017; Ritchie, 1994).

The pronounced effect of moisture content on air exchange is further illustrated by the correlations between CO_2 build-up/O_2 depletion and moisture content/differential pressure recorded near the reactive zone in experimental pile 2 (Fig. 8). The negative differential pressures observed in the hotspot of pile 2 (down to −25 Pa near December 2010; Fig. 7) appear to be slightly larger than the average negative differential pressure recorded in the hotspot of pile 3 (−15 Pa; Fig. 5) and may therefore be related to the slightly smaller particle size of waste rock in pile 2 compared to pile 3 (Table 1). Finally, the extent of O_2 depletion, CO_2 enrichment, and poregas pressure reduction relative to atmospheric conditions all decrease with increasing distance from the reactive waste rock 'hotspot' located near the top of the pile (Fig. 7), suggesting that advective atmospheric exchange to that hotspot may occur preferentially through the coarser basal regions of the pile.

The temperatures along instrumentation line 4 in experimental pile 2 were consistently higher than the air temperature, and the temperature gradient between the waste rock and the atmosphere gradually decreases as the distance of the sensor from the reactive waste rock 'hotspot' increases (Fig. 7). During the dry season, the temperature in the waste-rock pile slightly increases, whereas the temperature sensors recorded decreasing internal temperatures during the wet season. During the wet season, infiltrating water may have had the ability to moderate the temperatures inside the pile, but a previously discussed wetting front does not become apparent from the temperature data. In addition, water has a higher thermal conductivity than air, and dry waste rock may therefore be better insulating than wet waste rock. Therefore, the role of physical heterogeneities and moisture content variability on heat transfer processes in waste-rock piles, and their potential feedback on gas transport mechanisms (e.g., through thermal convection (Lahmira et al., 2017; Lefebvre et al., 2001b)), may be the topic of further research, for instance using reactive transport modeling. In summary, these results show that physicochemical heterogeneities of waste rock, combined with seasonal variations in moisture content, enforce strong and coupled controls on the gas- and heat transport processes that control the poregas distribution in waste-rock piles.

4. Conclusions

Analysis of the poregas composition of waste rock in five experimental waste-rock piles revealed temporally and spatially variable poregas compositions, temperatures, and pressures. Multiple and substantial zones with elevated temperatures (> 10 °C) and CO_2 levels (> 20,000 ppm) and significant O_2 depletion (< 15%) were observed in areas with fine-grained and reactive, high sulfide waste rock. The temperature and poregas composition profiles of the experimental waste-rock piles could not only be related to chemical reactivity (i.e. elevated sulfide content), and porosity of the waste rock (i.e. particle size), but also to seasonal variations in moisture content resulting from the balance between infiltration and evaporation of precipitation. Although a quantitative description of the isolated effects of aforementioned factors may require further (controlled) experiments or coupled reactive-transport models, this study demonstrates that *in-situ* monitoring of poregas pressures and O_2 and CO_2 profiles can provide insights into the weathering and drainage generation rates within waste-rock piles. Therefore, improved predictions of the environmental risks associated with waste rock weathering and drainage release may

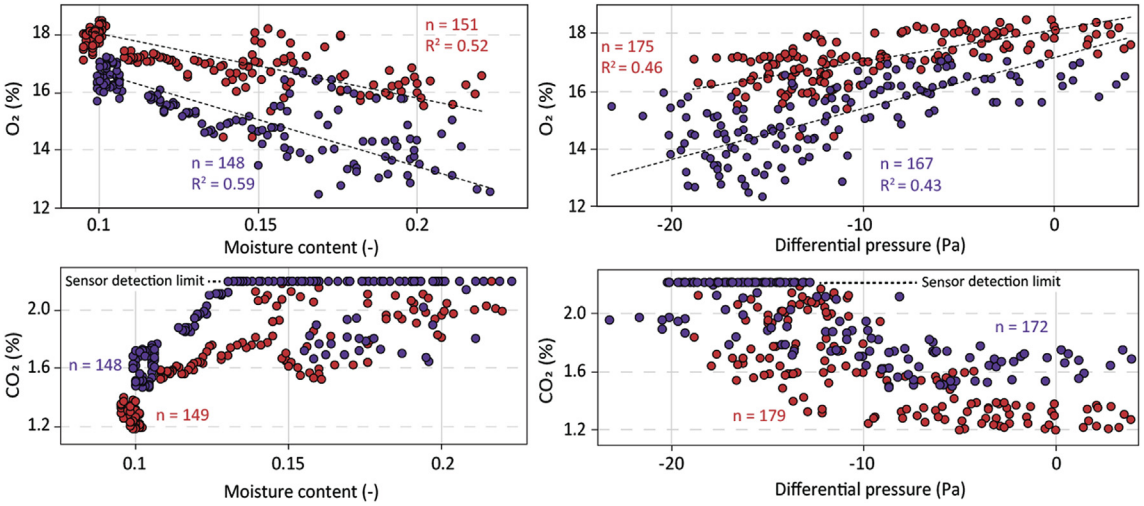

Fig. 8. Correlations between poregas composition and moisture content (left) and differential pressure (right) in waste rock near the reactive zone in experimental pile 2. The daily average poregas composition (O_2, top; CO_2, bottom) is plotted against waste rock moisture content and differential poregas pressure, recorded by sensors and at adjacent sampling ports. The color coding and measurement period between April 2010 and January 2011 is similar to in Fig. 7. Sample sizes and linear regression lines with coefficients of determination (R^2) for O_2 measurements are indicated; measurements exceeding the upper detection limit of the CO_2 sensor (~2.2%) are plotted at that limit. (For interpretation of the references to color in this figure legend, the reader is referred to the Web version of this article.)

benefit from continuing monitoring of *in-situ* poregas conditions in large-scale, heterogeneous waste-rock piles.

Disclosure

The authors declare no conflicts of interest.

Acknowledgements

We gratefully acknowledge the help of O. Singurindy, M. Lorca, H. Peterson, T. Hirsche, M. Javadi, S. Blackmore, K. Small, and C. Aranda with the installation of instrumentation, sample collection, and data processing. Financial support was provided by Compañia Minera Antamina S.A., the Natural Sciences and Engineering Research Council of Canada (NSERC; CRDPJ334909-2005), Teck Metals Limited's Applied Research and Technology Group, and a Canadian Foundation for Innovation grant (CFI) awarded to K.U. Mayer.

Appendix A. Supplementary data

Supplementary data to this article can be found online at https://doi.org/10.1016/j.apgeochem.2018.12.009.

References

Amos, R.T., Blowes, D.W., Smith, L., Sego, D.C., 2009. Measurement of wind-induced pressure gradients in a waste rock pile. Vadose Zone J. 8, 953–962.
Amos, R.T., Blowes, D.W., Bailey, B.L., Sego, D.C., Smith, L., Ritchie, A.I.M., 2015. Waste-rock hydrogeology and geochemistry. Appl. Geochem. 57, 140–156.
Birkham, T.K., Hendry, M.J., Wassenaar, L.I., Mendoza, C.A., Lee, E.S., 2003. Characterizing geochemical reactions in unsaturated mine waste-rock piles using gaseous O2, CO2, 12CO2, and 13CO2. Environ. Sci. Technol. 37, 496–501.
Blackmore, S., Smith, L., Mayer, K.U., Beckie, R.D., 2014. Comparison of unsaturated flow and solute transport through waste rock at two experimental scales using temporal moments and numerical modeling. J. Contam. Hydrol. 171, 49–65.
Blackmore, S., Vriens, B., Sorensen, M., Power, I., Smith, L., Hallam, S., Mayer, K.U., Beckie, R.D., 2018. Microbial and geochemical controls on waste rock weathering and drainage quality. Sci. Total Environ. 640–641, 1004–1014.
Chi, X., Amos, R.T., Stastna, M., Blowes, D.W., Sego, D.C., Smith, L., 2013. The Diavik waste rock project: implications of wind-induced gas transport. Appl. Geochem. 36, 246–255.
Dold, B., 2014. Evolution of acid mine drainage formation in sulphidic mine tailings. Minerals 4, 621–641.
Elberling, B., Nicholson, R.V., Scharer, J.M., 1994. A combined kinetic and diffusion model for pyrite oxidation in tailings: a change in controls with time. J. Hydrol. 157, 47–60.
Gerke, H.H., Molson, J.W., Frind, E.O., 1998. Modelling the effect of chemical heterogeneity on acidification and solute leaching in overburden mine spoils. J. Hydrol. 209, 166–185.
Harries, J.R., Ritchie, A.I.M., 1985. Poregas composition in waste rock dumps undergoing pyritic oxidation. Soil Sci. 140, 143–152.
Harries, J.R., Ritchie, A.I.M., 1981. The use of temperature profiles to estimate the pyritic oxidation rate in a waste rock dump from an opencut mine. Water Air Soil Pollut. 15, 405–423.
Harrison, B., Aranda, C., Sanchez, M., Vizconde, J., 2012. Waste rock management at the Antamina mine: overall management and data application in the face of continued expansion. In: Proceedings of the 9th International Conference on Acid Rock Drainage (ICARD), Ottawa, ON, Canada, pp. 1176–1187.
Lahmira, B., Lefebvre, R., 2015. Numerical modelling of transfer processes in a waste rock pile undergoing the temporal evolution of its heterogeneous material properties. Int. J. Min. Reclamat. Environ. 29, 499–520.
Lahmira, B., Lefebvre, R., Aubertin, M., Bussière, B., 2017. Effect of material variability and compacted layers on transfer processes in heterogeneous waste rock piles. J. Contam. Hydrol. 204, 66–78.
Lefebvre, R., Hockley, D., Smolensky, J., Gélinas, P., 2001a. Multiphase transfer processes in waste rock piles producing acid mine drainage. 1: conceptual model and system characterization. J. Contam. Hydrol. 52, 137–164.
Lefebvre, R., Hockley, D., Smolensky, J., Lamontagne, A., 2001b. Multiphase transfer processes in waste rock piles producing acid mine drainage: 2. Applications of numerical simulation. J. Contam. Hydrol. 52, 165–186.
Lefebvre, R., Lamontagne, A., Wels, C., 2001c. Numerical simulations of acid drainage in the sugar shack south rock pile, questa mine, New Mexico, USA. In: Proceedings of the 2nd Joint IAH-CNC and CGS Groundwater Specialty Conference - 54th Canadian Geotechnical Conference, pp. 1568–1570.
Linklater, C.M., Sinclair, D.J., Brown, P.L., 2005. Coupled chemistry and transport modelling of sulphidic waste rock dumps at the Aitik mine site, Sweden. Appl. Geochem. 20, 275–293.
Lorca, M.E., Mayer, K.U., Pedretti, D., Smith, L., Beckie, R.D., 2016. Spatial and temporal fluctuations of pore-gas composition in sulfidic mine waste rock. Vadose Zone J. 15. https://doi.org/10.2136/vzj2016.05.0039.
Love, D.A., Clark, A.H., Glover, J.K., 2004. The lithologic, stratigraphic, and structural setting of the giant Antamina copper-zinc skarn deposit, Ancash, Peru. Econ. Geol. 99, 887–916.
Malmström, M.E., Destouni, G., Banwart, S.A., Strömberg, B.H.E., 2000. Resolving the scale-dependence of mineral weathering rates. Environ. Sci. Technol. 34, 1375–1378.
Massmann, J., Farrier, D., 1992. Effects of atmospheric pressures on gas transport in the vadose zone. Water Resour. Res. 28, 777–791.
Molins, S., Mayer, K.U., 2007. Coupling between geochemical reactions and multicomponent gas and solute transport in unsaturated media: a reactive transport modeling study. Water Resour. Res. 43, W05435.
Ning, L., Zhang, Y., 1997. Onset of thermally induced gas convection in mine wastes. Int. J. Heat Mass Tran. 40, 2621–2636.
Nordstrom, D.K., Blowes, D.W., Ptacek, C.J., 2015. Hydrogeochemistry and microbiology of mine drainage: an update. Appl. Geochem. 57, 3–16.
Parbhakar-Fox, A., Lottermoser, B.G., 2015. A critical review of acid rock drainage prediction methods and practices. Miner. Eng. 82, 107–124.
Pedretti, D., Mayer, K.U., Beckie, R.D., 2017. Stochastic multicomponent reactive transport analysis of low quality drainage release from waste rock piles: controls of the spatial distribution of acid generating and neutralizing minerals. J. Contam. Hydrol. 201, 30–38.

Pham, N.H., Sego, D.C., Arenson, L.U., Blowes, D.W., Amos, R.T., Smith, L., 2013. The Diavik Waste Rock Project: measurement of the thermal regime of a waste-rock test pile in a permafrost environment. Appl. Geochem. 36, 234–245.
Qing, S., Yanful, E., 2010. Effect of water addition frequency on oxygen consumption in acid generating waste rock. J. Environ. Eng. 136, 691–700.
Ritchie, A.I.M., 1994. The waste-rock environment. In: Jambor, J.L., Blowes, D.W. (Eds.), Short Course Handbook on Environmental Geochemistry of Sulfide Mine-wastes. Mineralogical Association of Canada, pp. 133–161.
Ritchie, A.I.M., 2003. Oxidation and gas transport in piles of sulfidic material. In: Jambor, J.L., Blowes, D.W., Ritchie, A.I.M. (Eds.), Environmental Aspects of Mine Wastes, Short Course Series. Mineralogical Association of Canada, pp. 73–94.
Smith, L., Beckie, R.D., 2003. Hydrologic and geochemical transport processes in mine waste rock. In: Jambor, J.J.L., Blowes, D.W., Ritchie, A.I.M. (Eds.), Environmental Aspects of Mine Wastes, Short Course Series. Mineralogical Association of Canada, pp. 51–72.
Smith, L.J.D., Moncur, M.C., Neuner, M., Gupton, M., Blowes, D.W., Smith, L., Sego, D.C., 2013. The Diavik waste rock project: design, construction, and instrumentation of field-scale experimental waste-rock piles. Appl. Geochem. 36, 187–199.
Sracek, O., Gélinas, P., Lefebvre, R., Nicholson, R.V., 2006. Comparison of methods for the estimation of pyrite oxidation rate in a waste rock pile at Mine Doyon site, Quebec, Canada. J. Geochem. Explor. 91, 99–109.
Strömberg, B., Banwart, S., 1994. Kinetic modelling of geochemical processes at the Aitik mining waste rock site in northern Sweden. Appl. Geochem. 9, 583–595.
Strömberg, B., Banwart, S., 1999. Experimental study of acidity-consuming processes in mining waste rock: some influences of mineralogy and particle size. Appl. Geochem. 14, 1–16.
Thorstenson, D.C., Pollock, D.W., 1989. Gas transport in unsaturated porous media: multicomponent systems and the adequacy of Fick's law. Water Resour. Res. 25, 477–507.
Vriens, B., StArnault, M., Laurenzi, L., Smith, L., Mayer, K.U., Beckie, R.D., 2018. Localized sulfide oxidation limited by oxygen supply in a full-scale waste rock pile. Vadose Zone J. 17 (1), 180119.
Vriens, B., Peterson, H., Laurenzi, L., Smith, L., Aranda, C., Mayer, K.U., Beckie, R.D., 2019. Long-term monitoring of waste-rock weathering at Antamina, Peru. Chemosphere 215, 858–869.
Wels, C., Lefebvre, R., Robertson, A., 2003. An overview of prediction and control of air flow in acid-generating waste rock dumps. In: Proceedings of the 6th International Conference on Acid Rock Drainage (ICARD), Cairns, Australia, pp. 639–650.
Welty, J.R., Wicks, C.R., Wilson, R.E., 1984. Fundamentals of Momentum, Heat, and Mass Transfer, third ed. John Wiley & Sons, Inc., New York.
Yanful, E.K., Simms, P.H., Payant, S.C., 1999. Soil covers for controlling acid generation in mine tailings: a laboratory evaluation of the physics and geochemistry. Water Air Soil Pollut. 114, 347–375.